

Bonding of antimony on GaAs(110): A prototypical system for adsorption of column-V elements on III-V compounds

Perry Skeath,* C. Y. Su,[†] W. A. Harrison, I. Lindau, and W. E. Spicer
Stanford Electronics Laboratories, Stanford University, Stanford, California 94305
(Received 14 June 1982; revised manuscript received 16 February 1983)

It is shown that the atomic structure of column-V-element overlayers on GaAs(110) is in the form of a zigzag chain arrangement by a combination of detailed experimental investigation (using both photoemission electron spectroscopy and low-energy electron diffraction) and simple theoretical analysis. Antimony (Sb), used as a representative column-V element, spontaneously forms zigzag chains which are parallel to and in registry with the zigzag chains of the GaAs(110) surface when deposited at room temperature. The close lattice match between the size of the GaAs(110) surface unit cell and the zigzag chain constructed with Sb favors a near-ideal (dehybridized Sb orbitals in the Sb—Sb bonds) structure for the adatom chain when bonded to the substrate. The result is a new very-well-ordered atomic arrangement on the surface with two Sb atoms inside the GaAs(110) surface unit cell. From simple calculations, it is shown that the dehybridization of the states of the column-V atom in the zigzag chain structure results in a surprisingly narrow (~ 1.5 -eV) band of bonding p states, when compared to the ~ 12 -eV bandwidth of bonding p states in a linear chain. Strong evidence for this narrow band of Sb p states is shown in the photoemission data. Two schemes for attachment of the zigzag chain to the GaAs(110) surface are presented and their electronic structure is analyzed. This analysis shows that the states generated by the two attachment schemes fall in the same energy regions, and hence the present combination of photoemission data and simple theoretical analysis does not identify with certainty which scheme is the correct one. However, careful low-energy electron diffraction analysis by Kahn, Duke, and co-workers does favor one attachment scheme over the other. It is concluded that the combination of simple theoretical and detailed experimental approaches employed here are useful, in general, for determining the structure of column-V overlayers on III-V semiconductor surfaces.

I. INTRODUCTION

The bonding of column-V elements on the surfaces of III-V compounds is of interest for several reasons. First, an understanding of the column-V adatom to GaAs surface bond character (i.e., covalent versus metallic) and binding site gives insight about the electronic structure and chemistry of the semiconductor surface. Also, as will be shown below, well-ordered column-V-element overlayers can be obtained, in which case the structure (both atomic and electronic) of the overlayer can be studied. Lastly, information on the bonding of constituent elements to a crystal surface should contribute to our knowledge of the growth mechanism of the crystal.

It has been established that changes in surface valence-band electronic structure due to chemisorption of foreign atoms can be detected by proper photoemission experiments.¹ The GaAs(110) sur-

face [see Figs. 1(a)—1(c)] is most likely the best characterized and understood of all compound semiconductor surfaces and was thus chosen for these experiments. GaAs photoemission energy distribution curve (EDC) structure in the uppermost 5 eV of the valence band have proved particularly sensitive to changes in surface conditions²; thus, it is anticipated that a careful photoemission electron spectroscopy (PES) study of the top 5 eV of the valence band is essential for any understanding of the bonding of the column-V atoms to the surface. Low-energy electron diffraction (LEED) data provide essential complementary information, which characterizes the atomic structure of the ordered surface.

The technique of molecular-beam epitaxy³ (MBE) for growth of epitaxial layers on III-V compound semiconductors should be easily applied for investigations of crystal-growth mechanisms on an atomic level at the crystal surface. With the exception of the work by Bachrach,⁴ who studied Al and Ga on

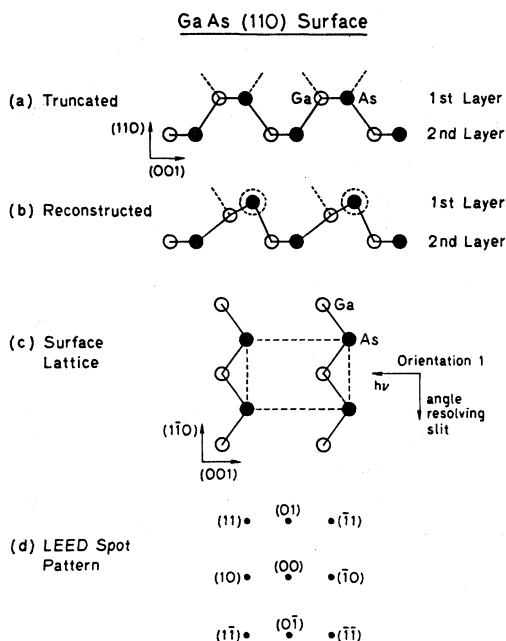


FIG. 1. Schematic illustrations of the GaAs(110) direct and reciprocal surface lattices. (a) Side view of the "ideal" truncated (unreconstructed) surface lattice, with dashed lines indicating broken bonds of sp^3 character. (b) Side view of the reconstructed (110) surface lattice always found on GaAs. The character of the nonbonding states (indicated with dashed line) changes with the reconstruction such that there is an empty p -like state on the Ga atom and a filled s -like lone pair on the As atom. Note that the reconstruction is consistent with a planar (sp^2) configuration preferred by the column-III elements and an atomiclike (dehybridized) configuration preferred by the column-V elements. (c) Top view of the surface lattice, showing only the first layer. The surface atoms are arranged in zigzag chains, with a rectangular unit cell containing one Ga and one As atom. The azimuthal angle of the incident light's propagating direction (labeled $h\nu$) and angle-resolving slit, which are always 90° apart from each other, are shown for orientation 1. (d) The reciprocal of the surface lattice shown in (c). The LEED diffraction beams referred to in this work are identified by their corresponding reciprocal lattice point.

GaAs(110), MBE techniques have not been used to uncover the basic mechanism by which adsorbed atoms or molecules are bound into lattice sites. (That is, where are the preferred adsorption sites for Ga or As on a specific GaAs surface? How does the adsorbed layer get into epitaxial alignment if these are not GaAs lattice sites?)

For the study of column-V elements (Sb) adsorbed on GaAs(110), the above techniques (PES, LEED, and MBE) are combined. After giving the impor-

tant experimental considerations, PES and LEED data are presented. LEED I - V profiles are shown for two integral order diffraction beams as a function of coverage. PES was used to monitor both the core levels (Ga $3d$, As $3d$, and Sb $4d$) and valence-band electronic structure. Data are first presented as a function of Sb coverage. Oxidation data for a Sb monolayer on GaAs(110) are shown. The remainder of the PES data is devoted to a study of the Sb-induced valence states by both angle-integrated and angle-resolved PES.

A list of characteristics of the Sb overlayer is assembled at the start of Sec. IV. Structural models are then proposed based on these characteristics and on the chemistry of the GaAs(110) surface. The electronic states associated with these models are calculated by a simple linear combination of atomic orbitals (LCAO) method. These calculated states are then compared to those observed in the PES data. It is concluded that the zigzag chain models do account for the experimentally observed characteristics of the Sb overlayer. The results of other experimental work on column-V element adsorption on GaAs(110) are also discussed.

II. EXPERIMENTAL CONSIDERATIONS

The photoemission portion of this investigation was done using continuously variable, nearly monochromatic light from the 4° beam line ($60 \text{ eV} \leq h\nu \leq 500 \text{ eV}$) and from the 8° beam line ($10.2 \text{ eV} \leq h\nu \leq 32 \text{ eV}$) at the Stanford Synchrotron Radiation Laboratory.⁵ The monochromator design for these beam lines is such that the inherent polarization of the synchrotron light in the horizontal plane is preserved. The experimental chamber layout (see Fig. 2) is such that the light impinges on the sample surface at near-grazing incidence (76° from the surface normal); thus, the electric field of the light at the surface is nearly perpendicular to the surface (A is 14° from the surface normal—mainly p polarized). A PHI 15-255G double-pass cylindrical-mirror analyzer (CMA) with axis parallel to the sample surface normal was used to obtain photoelectron and Auger electron energy spectra. The CMA collects electrons within a polar angle window of $42.3^\circ \pm 6^\circ$ and essentially integrates over azimuthal angles. During part of the photoemission experiments, a slit was positioned in front of the CMA to mask all but a 15° segment of the azimuthal angles. The slit was centered on a vertical axis in the chamber (perpendicular to the horizontal plane of Fig. 2) below the CMA axis.

The GaAs crystals were nearly degenerately doped p -type ($2 \times 10^{18} \text{ cm}^{-3}$ Zn, Laser Diode) and n -type ($5 \times 10^{17} \text{ cm}^{-3}$ Sn, Varian). Clean GaAs(110)

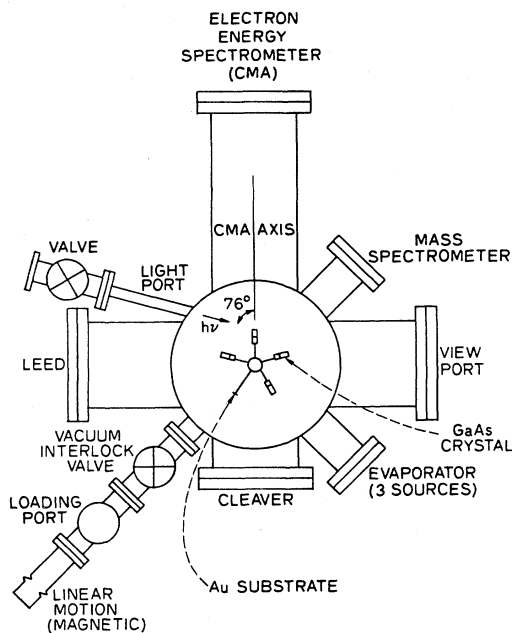


FIG. 2. Schematic illustration of the experimental apparatus. Single crystal GaAs cleaving bars are mounted on a rotatable carousel in the center of the vacuum chamber. A metal (Au) substrate and a quartz thickness monitor (not shown) were also located on the carousel. After cleaving in ultrahigh vacuum ($\leq 10^{-10}$ Torr), characterization of the surface can be done with the CMA (used for photoemission electron spectroscopy and Auger electron spectroscopy) or the LEED apparatus. Light impinges on the sample surface at near-grazing incidence. An evaporator flange containing three shuttered evaporators and a second crystal-thickness monitor was used as a source of Sb, Al, Ga, In, or Au for deposition on GaAs. Transfer of samples into and out of the chamber was possible without breaking vacuum by use of a vacuum interlock. The chamber was designed by Dr. P. Pianetta (Hewlett-Packard Corp., Palo Alto, California).

surfaces were prepared by cleaving under vacuum. Surfaces with low defect density can be produced by this technique.^{2,6}

Sb was deposited on the sample by evaporating from a shuttered bead or quartz crucible source. The evaporation rate was determined by Sloan crystal-thickness monitors mounted alongside the evaporators and on the sample carousel, and the amount deposited was calculated from the rate and exposure time. The evaporation sources and deposition techniques are described in more detail elsewhere.⁷ We define monolayer (ML) coverage to be the same as the number of atoms in the surface lattice of GaAs(110) for convenience (0.89×10^{15} atoms/cm²). Sample exposures to antimony (Sb) are given in terms of a dosage (in units of 10^{15} atoms

incident/cm²) instead of coverage, in consideration of a sticking coefficient of Sb on GaAs which may be less than unity. These dosages are determined by referencing to an Sb-covered thickness monitor, and thus they assume a unity sticking coefficient for Sb on Sb. Thus, the absolute dosages may be in error by a factor equal to the reciprocal of the sticking coefficient of Sb on Sb, but relative dosages are well determined.

Calibration of the actual Sb coverage was possible in the core-level PES data from the ratio of Sb 4*d* to Ga 3*d* peak areas. For clean cleaved GaSb(110), this ratio is 1.7 at a photon energy of 110 eV. Taking into account that an Sb overlayer has about twice the Sb atoms per unit volume as GaSb, ignoring interdiffusion, and assuming an inelastic scattering probability that is constant inside the solid and drops abruptly to zero outside the surface,⁸ the formula

$$\frac{A_{\text{Sb}}}{A_{\text{Ga}}} = 3.4(e^{+d/L} - 1)$$

was used to determine the coverage. Here, A_x is the area under the core-level peak of element x , L is the scattering length (assumed the same in Sb, GaAs, and GaSb), and d is the Sb layer thickness.

LEED beam intensity versus primary beam energy (I - V) data were obtained using a standard Varian four-grid LEED optics (shielded by μ metal) and a Gamma Scientific T-5 spot photometer. Only a single scan of each diffraction beam was done; thus, only the gross features of each I - V curve are reliable and the details are probably not accurate. In all cases the data are normalized to the beam current.

III. RESULTS

A. Determination of order in Sb overlayers

The 1×1 LEED pattern was preserved along with the mirror plane symmetry after 1×10^5 cm⁻² Sb adsorption at room temperature.⁹ Thus the size and basic symmetry of the surface unit cell was unchanged by 1 ML Sb adsorption. To determine if a change in atomic structure within the surface unit cell had occurred, LEED I - V data were obtained before and after Sb deposition. Changes in the relative diffraction spot intensities indicated the binding of Sb to a specific site (or sites) within the GaAs surface unit cell resulting in an ordered Sb overlayer.⁹

In a separate experiment (at Stanford University, in which we gratefully acknowledge collaboration with A. Kahn of Princeton University), LEED I - V profiles for the $(\bar{1}0)$ and $(\bar{1}\bar{1})$ beams were obtained as a function of Sb dosage (see Figs. 3 and 4). At

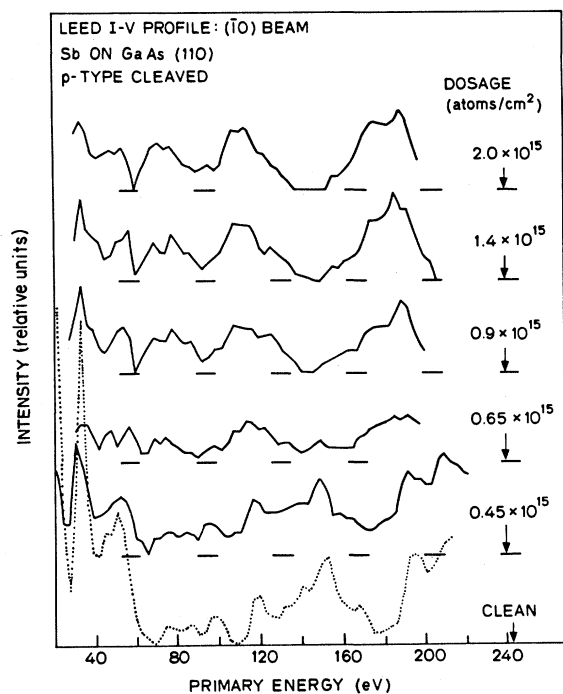


FIG. 3. Single-scan LEED I - V profiles of the $(\bar{1}0)$ beam vs Sb dosage. The baseline for each profile is indicated by a dashed line, with an arrow to show what baseline corresponds to a given dosage. Note that the profiles are in relative units (no vertical scaling factors) and normalized to the beam current after subtracting off the background intensity.

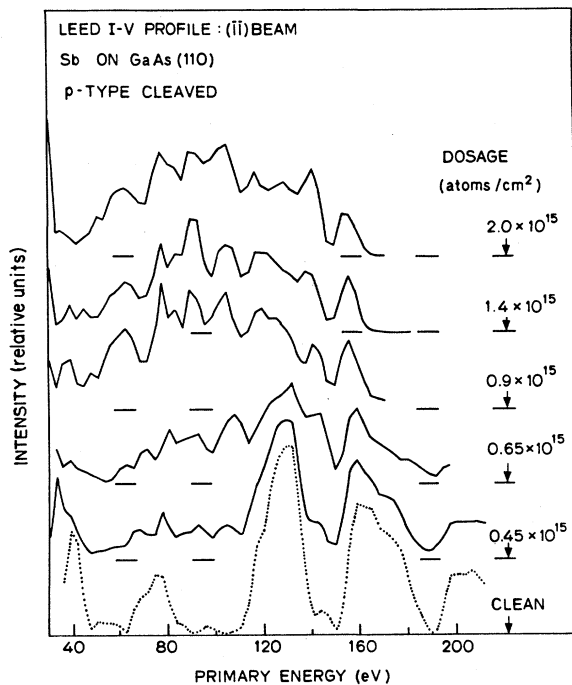


FIG. 4. Single-scan LEED I - V profiles of the $(\bar{1}\bar{1})$ beam vs Sb dosage.

the lowest dosage (0.45×10^{15} Sb atoms/cm²), there is evidence of damping or smearing of the I - V structure, particularly at very low energies (≤ 40 eV), and slight indication of new structure. The I - V profiles are markedly changed by the second Sb dose (0.65×10^{15} atoms/cm² total) with the appearance of prominent new structure in the I - V profiles. The new I - V profiles are essentially constant in the dosage range 0.9 – 2.0×10^{15} atoms/cm². A larger dosage of 5×10^{15} Sb atoms/cm² was made, from which it was observed by eye that the I - V profiles were very much the same as for the 1 – 2×10^{15} dosage range, although the background intensity was much greater. Thus there is only a single ordered phase, 1–2 ML in thickness. The comparable diffraction intensities (peak heights in the I - V profiles) of the $(\bar{1}0)$ beam for clean and Sb-covered surfaces indicate that some asymmetry or deviation from a “truncated diamond lattice” configuration¹⁰ remains after depositing Sb.

More recently, Carelli and Kahn, and co-workers, have shown that the ordered overlayer is 1 ML thick, which forms islands at submonolayer coverage.¹¹ It was concluded from their work that the average island size was quite small (in the 10–100 Å range) compared to the coherence length of the beam (300–400 Å). The diffraction beam broadening, which indicated island formation, did not display any obvious anisotropy and disappeared at monolayer Sb coverage.

B. Chemical states of adsorbed and oxidized Sb

Chemisorbed Sb on GaAs was studied by soft-x-ray photoemission spectroscopy (SXPS) as successively greater amounts of Sb were deposited (see Fig. 5). Emission from the Sb 4*d* core level increased dramatically after a total dose of 0.4×10^{15} cm⁻², suggesting that the sticking coefficient of Sb on this surface had increased after the first two exposures. For total dosages of 0.7×10^{15} cm⁻² and higher, the separation between Ga 3*d* and As 3*d* core levels began to increase: The Ga 3*d* remained fixed at a total shift of 0.2–0.3 eV, while the As 3*d* shift increased monotonically to a maximum of 0.6 eV (toward higher binding energy). Since this effect was seen mainly at higher coverages, it indicates a small amount of diffusion of Ga and As into the Sb overlayer. Changes in Ga 3*d* and As 3*d* core-level widths were ≤ 0.15 eV throughout the series of Sb depositions (resolution is equal to 0.25 eV). The valence-band emission resembles a superposition of bulk Sb emission on GaAs emission after a dosage of 1.4×10^{15} cm⁻², although some extra emission is apparent near the valence-band maximum (VBM).

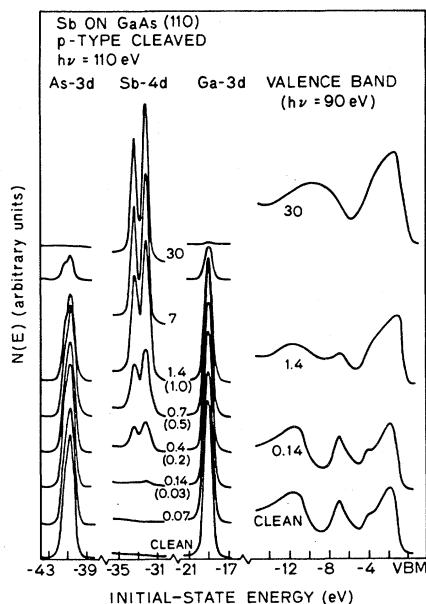


FIG. 5. Core-level ($h\nu=110$ eV) and valence-band ($h\nu=90$ eV) photoemission data for a sequence of Sb exposures on GaAs(110). Sb dosages are shown in units of 10^{15} incident atoms/cm² and, where important, the actual coverage is given in parentheses (10^{15} atoms adsorbed/cm²). Note the increase in the resolution of the Sb 4*d* spin-orbit splitting at high coverage ($\geq 7 \times 10^{15}$ atoms/cm²) compared to low coverage ($\leq 1.0 \times 10^{15}$). CMA resolution is 0.25 eV.

At high coverages ($> 7 \times 10^{15}$ cm⁻² dosage), the Sb 4*d* spin-orbit splitting is much more well defined, although no appreciable broadening or shifting (≥ 0.2 eV) of the Sb 4*d* core level as a whole was observed throughout the series of exposures. Since shortening of the Sb 4*d* core-hole lifetime is not expected to be greater in the monolayer than in bulk Sb, we conclude that the less well-resolved spin-orbit splitting at low coverage is due to the superposition of two or more Sb 4*d* core levels with a small chemical shift between them, and we note that it occurs at submonolayer as well as monolayer coverage.

A single monolayer of Sb on GaAs(110) was given a series of exposures to oxygen as another means of characterizing the ordered overlayer. Following deposition of the Sb, sharpening of the As 3*d* core level (judged by the increased visibility of the spin-orbit splitting) was particularly noticeable on this surface (see Fig. 6). This suggests that the surface chemical shift of the outermost As atoms¹² has been reduced by the bonding of Sb to the surface. After a 10^7 L O₂ exposure (1 L = 1 langmuir = 10^{-6} Torr sec), chemically shifted Sb 4*d* emission is quite clear.

For comparison to the oxidation of bulk Sb, a

thick (> 50 ML) Sb film prepared by the same techniques was given a single oxygen exposure of 10^7 L. The oxygen uptake by "bulk" Sb was far greater than that of the ordered monolayer of Sb on GaAs(110) for equal exposures and exhibited a single very-well-defined shifted component of the Sb 4*d* core level (see Fig. 6), most likely due to the formation of Sb₂O₃. The oxygen uptake by the Sb monolayer after a 10^9 L O₂ exposure is still less than that of the "bulk" Sb film after a 10^7 L O₂ exposure, with no predominance of a single chemically shifted Sb 4*d* core level in the Sb monolayer.

The oxidation of the Sb monolayer can also be compared to the oxidation of GaAs and GaSb(110). For exposures of bare GaAs(110) to greater than 10^7 L O₂, a single chemically shifted As 3*d* peak is clearly resolved such that, at 10^7 L O₂, it is estimated that oxygen is bonded to $\sim 17\%$ of the surface As atoms and, at 10^9 L O₂, the estimate is $\sim 50\%$.¹³ With the use of the same technique of comparing the area under the chemically shifted versus unshifted Sb 4*d* core level, roughly the same oxygen uptake by the Sb monolayer is seen for equal exposure to oxygen, but without resolving a single chemical shift. It should also be noted that oxygen uptake by the GaAs is significantly reduced by the Sb monolayer.

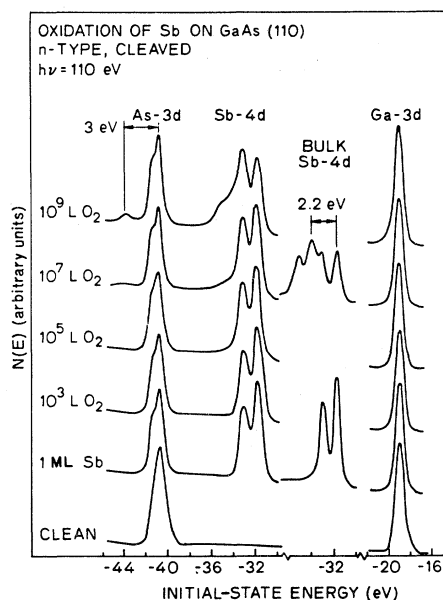


FIG. 6. Core-level spectra for the oxidation of an Sb monolayer on GaAs(110) and of "bulk" Sb. The Ga 3*d* core levels have been aligned at 19 eV binding energy to eliminate shifts of the spectra due to changes in Fermi energy pinning. The "bulk" Sb 4*d* core level is shown only for the clean surface and for 10^7 L O₂ exposure, to the right of the corresponding "monolayer" Sb 4*d* core level.

In contrast to GaAs, the oxidation of GaSb proceeds directly to bulk oxide formation.¹⁴ Comparing the GaSb data to the oxidation data for "bulk" Sb, it is clear that the oxygen uptake by the "bulk" Sb is slightly faster and that the charge transfer from the Sb (which is related to the oxidation state) is essentially the same in the two cases. Most interestingly, the oxygen uptake of the Sb monolayer on GaAs(110) is *slower* than that of bare GaSb(110); this suggests that oxygen more easily disrupts the GaSb surface than the Sb monolayer on GaAs.

The oxygen-induced valence-band structure of the Sb monolayer and "bulk" Sb was measured by PES during the same experiment. Comparison of the oxidized (10^7 L) bulk Sb to the monolayer Sb on GaAs(110) at the maximum exposure (10^9 L) again reveals differences between these two cases (see Fig. 7). The oxygen-induced structure of the "bulk" Sb sample bears a strong resemblance to that seen in the oxidation of a thick As film, which Su *et al.* associated with As_2O_3 formation.¹³ The oxygen-induced structure at high binding energy is particularly important in identifying the oxide species. The distinct shoulder at -7 eV in the oxidized "bulk" Sb curve, which is tentatively associated with Sb_2O_3 formation, is not seen in the oxidized Sb monolayer valence band.

C. Valence electronic states of Sb on GaAs(110)

The GaAs and Sb overlayer valence bands were given a more detailed examination by photoemission electron spectroscopy using lower photon energies, where higher resolution and band-structure information are more easily available. A single deposition

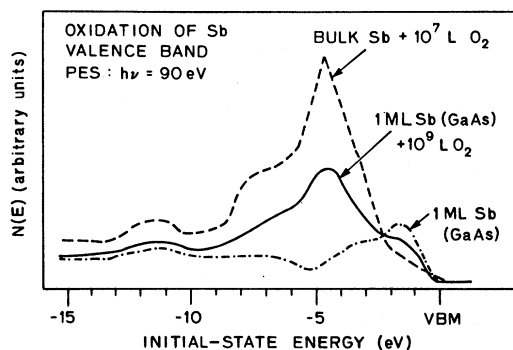


FIG. 7. Valence-band spectra corresponding to the core-level spectra of Fig. 6 for the unoxidized Sb monolayer (dot-dash), the Sb monolayer after exposure to 10^9 L O_2 (solid), and "bulk" Sb after exposure to 10^7 L O_2 (dash).

of Sb was made on a *p*-type GaAs(110) surface which displayed very sharp EDC structure (see Fig. 8). The appearance of the peak -1.5 eV below the GaAs VBM and disappearance of the -2 -eV peak is clearly seen following a dosage of $1.6 \times 10^{15} \text{ cm}^{-2}$ Sb. A difference curve, obtained by subtracting a scaled "clean-surface" EDC from the "Sb-covered" curve, was obtained to emphasize changes in the surface electronic structure. The difference curve bears some resemblance to the "bulk" Sb (30 Å thick, non-crystalline) EDC, but with a sharp notch at -2 eV, which may be due to the loss of the "clean-surface" GaAs EDC peak at that position. It should also be noted that some evidence of peaks at -4 and -3 eV remains in the difference curve. This may indicate either a slight change in the GaAs states at these energies or new Sb-derived states. Consistent with the LEED data (Figs. 3 and 4), only a single set of new valence-band features was observed in the coverage range from 0 to ~ 3 ML.⁹

The Fermi energy (E_F) was found to shift from 0.25 eV above the VBM on the clean surface to 0.55 eV above the VBM after depositing Sb (see Fig. 8), just above the emission associated with the Sb over-

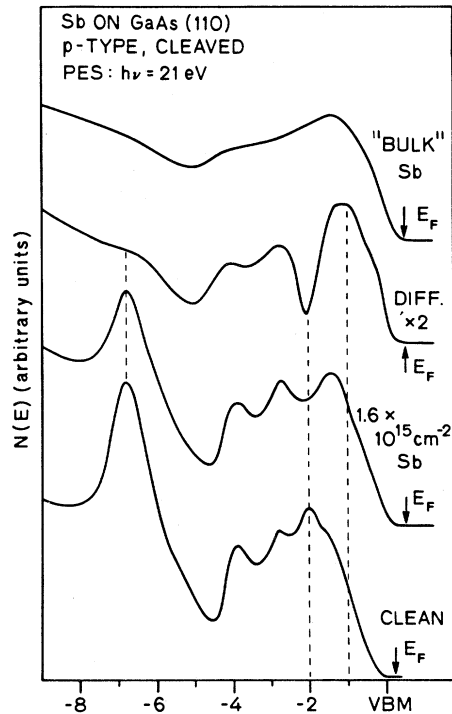


FIG. 8. PES valence-band EDC's (azimuthal angle-integrated) for clean and Sb-covered GaAs(110) with photon energy of 21 eV. The difference curve has been multiplied by 2, and a "bulk" Sb EDC has been included for comparison.

layer on GaAs(110), suggesting that both ordered (first monolayer) and disordered (second or more monolayers) phases of the Sb overlayer are semiconducting. Crystalline Sb is thought to be semimetallic,¹⁵ while amorphous Sb is semiconducting.¹⁶

To identify and characterize these new states and to separate their emission from that of Sb, which is not in an ordered phase, it is desirable to examine EDC's at monolayer Sb coverage (or submonolayer coverage, considering the island formation seen by Carelli and Kahn¹¹) for several photon energies. Both azimuthal angle-integrated and angle-resolved valence band EDC's were obtained in the photon energy range 15–28 eV for coverages of ~ 0.3 and ≥ 2 ML, with three different sample orientations identified as 2, 3, and 4. Referring to Fig. 1(c), each succeeding orientation involves a rotation of the crystal by 90° such that orientation 4 has the light's propagation direction (arrow labeled $h\nu$) pointing "up" in the $[\bar{1}10]$ direction. The $h\nu$ arrow also denotes the direction toward which the \vec{A} vector is tilted by $\sim 15^\circ$ from the surface normal, or $[110]$, axis.

Data with orientation 4 will be used as an example. Both azimuthal angle-integrated EDC's and difference curves were obtained at photon energies of 21, 25 (Fig. 9), and 28 eV. The clean-surface upper-valence-band EDC structure between -4 eV and the VBM varied markedly with photon energy,

yet the difference curves for 0.3 ML Sb coverage were relatively similar. Difference curves at all three photon energies show a prominent peak approximately 0.5 eV below the GaAs VBM and a valley at -2 eV. The position of the 0.5-eV peak varied only slightly (~ 0.15 eV) between 21 and 28 eV at this coverage. The valley at -2 eV was also seen for the other sample orientations and at higher coverages (as an example, compare to Fig. 8). At higher coverages ($\Theta \geq 2$ ML, Fig. 9), the difference curves bear a much stronger resemblance to "bulk" Sb. The structure of sharp peaks and valleys seen at lower coverage ($\Theta \sim 0.3$ ML) is replaced by broader emission, consistent with the disordered state of deposited Sb in excess of 1 ML.

More detailed information on the states associated with the GaAs-Sb interface can be obtained by using angle-resolved photoemission electron spectroscopy (ARPES), in which the azimuthal as well as the polar angle of photoelectrons sampled is constrained (sampling a much smaller region of both the surface and bulk Brillouin zone).

ARPES data were obtained from the same surface used for the azimuthal angle-integrated PES data for orientations 2, 3, and 4. (See Fig. 10 for electron

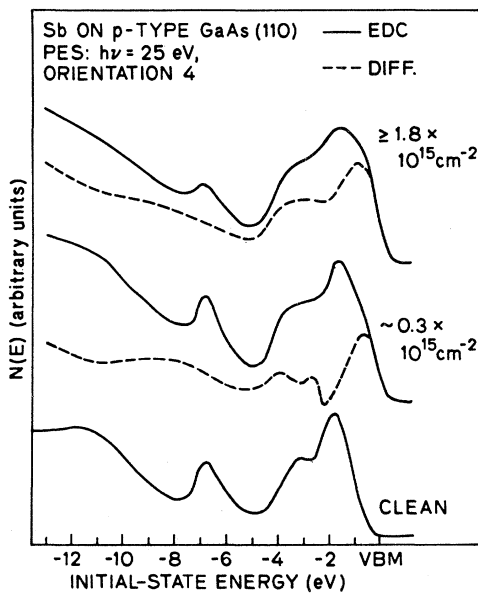


FIG. 9. Azimuthal angle-integrated EDC's (solid) for clean GaAs(110), ~ 0.3 ML, and ~ 2 ML Sb coverage using a photon energy of 25 eV, with difference curves (dashed). Orientation 4 was used, with CMA resolution equal to 0.15 eV. Note change in horizontal scale.

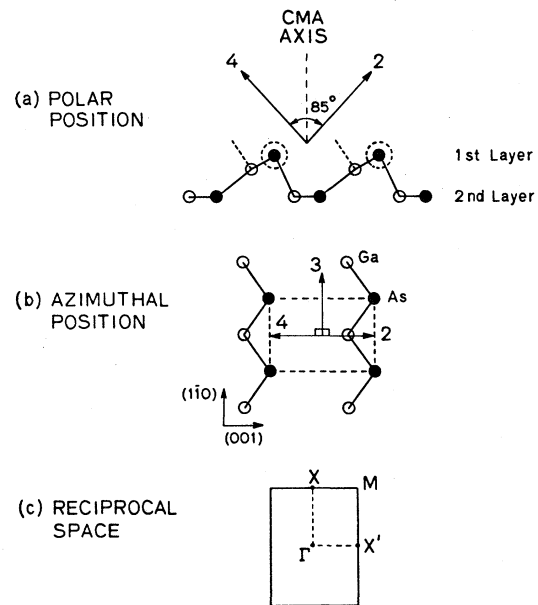


FIG. 10. Schematic illustration of the angle-resolving slit position with respect to the crystal surface. (a) The polar angle [CMA or $[110]$ axis is equal to 0°] is fixed at $42.6^\circ \pm 6^\circ$. Orientations 2 and 4 have the detector in the plane of the diagram. (b) The azimuthal position of the detector for orientations 2–4. (c) The unit cell of the reciprocal $[110]$ surface lattice, showing principal symmetry points.

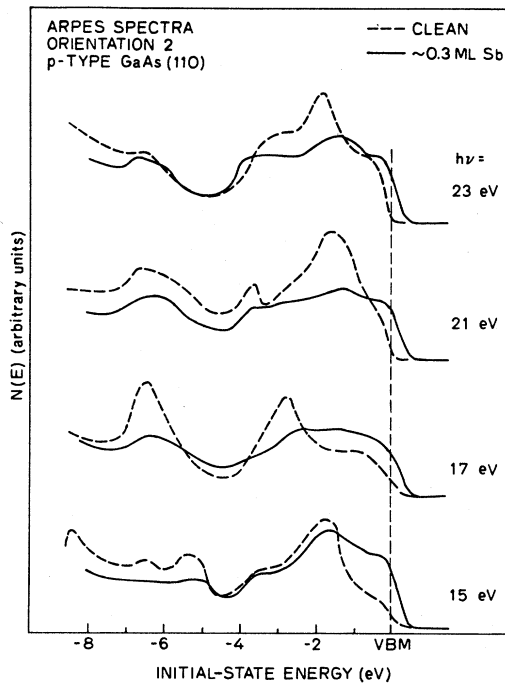


FIG. 11. Angle-resolved PES (ARPES) EDC's for orientation 2 before (dashed) and after (solid) deposition of ~ 0.3 ML Sb. Each 0.3 ML Sb curve has been normalized to the beam current of the corresponding "clean" curve. CMA resolution is 0.25 eV.

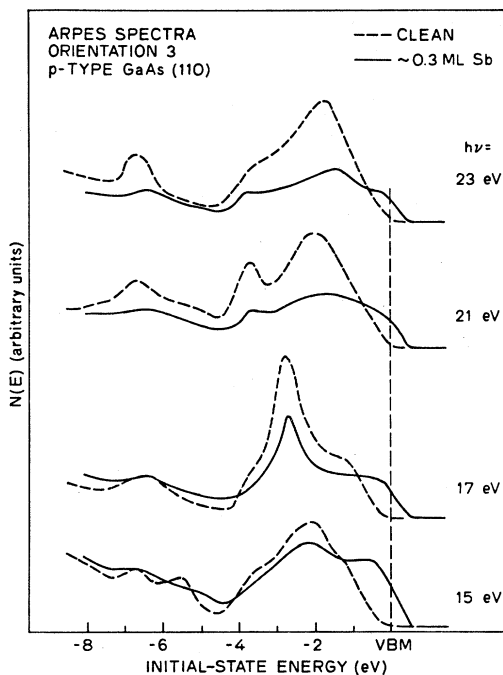


FIG. 12. Angle-resolved ARPES EDC's for orientation 3 before (dashed) and after (solid) deposition of ~ 0.3 ML Sb. Each 0.3 ML Sb curve has been normalized to the beam current of the corresponding "clean" curve. CMA resolution is 0.25 eV.

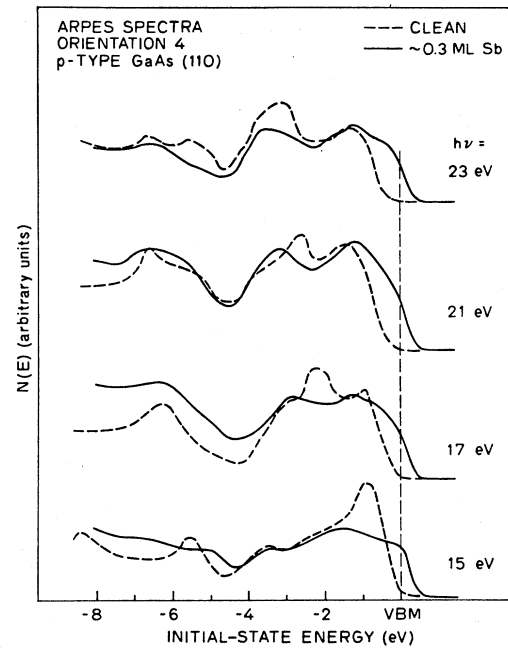


FIG. 13. Angle-resolved ARPES EDC's for orientation 4 before (dashed) and after (solid) deposition of ~ 0.3 ML Sb. Each 0.3 ML Sb curve has been normalized to the beam current of the corresponding "clean" curve. CMA resolution is 0.25 eV.

analyzer positions; the principle variation is in the azimuth of the electron analyzer.) Taking the (001) direction as 0° azimuthally [see Fig. 10(b)] with increasing angle counterclockwise, orientation 2 has the angle-resolving analyzer slit centered at 0° , orientation 3 at 90° , and orientation 4 at 180° . ARPES data were obtained at photon energies of 15, 17, 21, and 23 eV, so as to be able to observe any dispersion of states associated with the Sb-GaAs(110) interface.

The ARPES data for ~ 0.3 ML Sb coverage is overlaid on each of the clean-surface spectra (after normalization to synchrotron electron-beam current of the clean-surface spectra) in Figs. 11–13 for comparison. There are several general trends in the changes in the angle-resolved energy distribution core (AREDC) structure associated with Sb adsorption. First, the attenuation of much of the sharp AREDC structure (seen with the clean surface) is in excess of what would be expected from any reasonable escape-depth considerations. The states associated with these strongly attenuated EDC structures are apparently surface sensitive. Second, there is a strong increase in emission near the VBM, as was seen previously in the azimuthally integrated EDC's. This new emission near the VBM, a prominent shoulder, does not show any marked variation in structure with either photon energy or orientation of

the angle-resolving slit. Third, there is no strong evidence of other prominent new states. The Sb-induced states seen in the azimuthal angle-integrated difference curves between -2.5 and -4 eV apparently do not exhibit strong emission in the symmetry directions used for the AREDC's. It should be emphasized again here that the data in Figs. 9 and 11–13 are all taken from the same surface.

Since the strong Sb-induced emission near the VBM does not appear to vary markedly in structure from one orientation to another, it is desirable to also measure how this angle-resolved emission varies in *absolute* magnitude as a function of analyzer orientation. Variation of absolute magnitude can indicate the orientation of the Sb–Sb or Sb–GaAs bonds. For this purpose, the area under this emission *above* the bulk GaAs VBM was measured for each of the 0.3 ML EDC's. The absolute magnitudes of this averaged (areas from all four photon energies summed for each orientation) and normalized (to synchrotron beam current and to the corresponding angle-integrated emission) Sb-induced emission were found to be different: Orientation 3 had an emission area $1.08\times$ that of orientation 2, while orientation 4 had emission area $1.34\times$ that of orientation 2. Thus there is some asymmetry of the Sb-induced emission about the surface normal within the mirror plane of the surface unit cell. Further interpretation will be made with reference to the Sb overlayer models in the discussion section.

van Laar *et al.*¹⁷ have performed angular-resolved photoemission and low-energy electron-loss measurements on GaAs(110) with In, N, P, and As overlayers. As a general feature, concerning the lack of change in EDC structure seen by van Laar *et al.* following P and As deposition, we note that some complications may have arisen from the “cracking of AsH_3 or Ph_3 ” technique used by van Laar *et al.* to deposit As and P.

Constant final state (CFS) photoemission spectroscopy¹⁸ has been found to be useful for observing a sharp transition from the Ga 3*d* core level to an empty state near the GaAs conduction-band minimum. Experimental evidence indicates that the empty state is localized on the surface Ga atoms (with Ga 3*d* core hole) and is excitonic in nature, with bonding energy ~ 0.5 eV.¹⁹ This transition is notably stronger in GaSb than GaAs and, for this reason, the “excitonic” transition was monitored on both GaAs and GaSb(110) as Sb was deposited. The results were essentially the same, and thus only the Sb on GaSb data (which give better signal-to-noise ratios) are presented here. The “excitonic” transition appears as a doublet at 19.0- and 19.5-eV photon energy due to the spin-orbit splitting of the Ga 3*d* core level (see Fig. 14). There was a notable

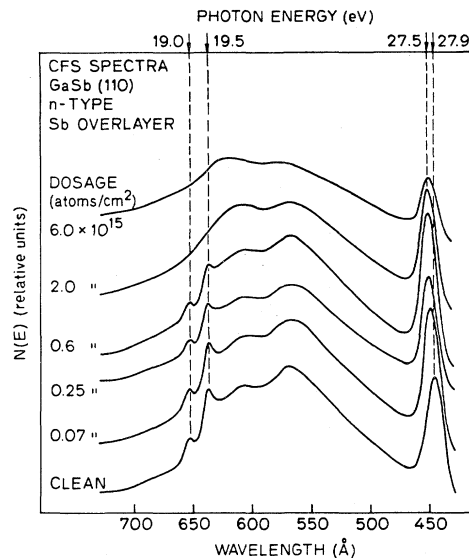


FIG. 14. Effect of room-temperature deposition of Sb on the “excitonic” transition (seen at 19.0 and 19.5 eV photon energy) thought to be from the Ga 3*d* core level into the empty Ga *p* state [C. A. Swarts *et al.* (Ref. 20)] on the GaSb(110) surface. Note the lack of shift in the “excitonic” transition and its extinction at 2×10^{15} (~ 2 ML) coverage. The sharp peak on the right is the Ga 3*d* core level which shifts from 27.9 to 27.5 eV due to band bending. A final state energy of 4 eV above the vacuum level was used.

damping of the excitonic transition after a 0.6×10^{15} Sb atoms/cm² dosage (~ 0.5 ML coverage), and the transition is completely gone after a 2×10^{15} Sb atoms/cm² dosage (~ 2 ML). A similar extinction of the excitonic transition occurred after a dosage of 1×10^{15} cm⁻² Sb on GaAs(110). This indicates that the bonding of Sb to the surface strongly perturbs the states at the surface, consistent with the previous data.

IV. DISCUSSION

A. Characteristics of the Sb overlayer

The characteristics of the Sb overlayer on GaAs(110) derived from this work may be summarized as follows:

- (1) Sb forms a well-ordered overlayer in registry with the GaAs(110) surface lattice when deposited at room temperature.
- (2) The size (1×1) and mirror symmetry of the surface unit cell are preserved after Sb deposition.
- (3) Only a single-ordered phase of the Sb overlayer, limited to the first monolayer or two of Sb deposited, was observed after deposition at room temperature for coverages ranging from 0.25 to 5

ML (result obtained at Stanford University in collaboration with A. Kahn of Princeton University).

(4) The dominant new valence-band photoemission peak associated with Sb absorption is located at 0.5–1.0 eV below the GaAs VBM.

(5) Some electronic states associated with the GaAs are strongly perturbed by the Sb overlayer. Furthermore, the Sb monolayer is likely to be bonded to both the surface Ga and As atoms, based on the apparent reduction in Ga $3d$ and As $3d$ surface chemical shift.

(6) The ordered Sb monolayer has an even number of Sb atoms (probably two atoms) per unit cell and is semiconducting. At least two chemically distinct states of Sb are always present in the coverage range between 0 and 2 ML.

(7) The Sb monolayer resists oxidation compared to “bulk” Sb, cleaved GaSb(110), or cleaved GaAs(110).

Carelli and Kahn¹¹ subsequently reproduced points 1–3 and deduced that there were two atoms per unit cell in the ordered overlayer. They further demonstrated that (i) annealing at sufficiently high temperatures ($\geq 250^\circ\text{C}$) desorbs any Sb that is in excess of 1 ML, leaving only a monolayer of Sb in the same ordered phase seen before annealing, and (ii) island formation occurs at submonolayer coverage.

These characteristics taken as a whole suggest that the ordered Sb monolayer is quite stable both structurally and chemically. It should be noted that there is self-consistency in the data since, bringing in a second Sb atom per unit cell, one is able to put all Sb p electrons in σ or strongly bound states (as will be shown below), producing a configuration that is much more stable electronically. The increased resistance of the ordered Sb monolayer to oxidation could be related either to a lack of weakly bound or nonbonding electrons in the ordered Sb monolayer, and/or to steric hindrance of the dissociation of O_2 . In the following development of models for Sb monolayers, an absence of weakly bound or nonbonding electrons will be taken to be an essential element.

B. Chemistry of Sb and GaAs(110)

It is necessary to first develop some general guidelines for the chemistry of both Sb and the GaAs(110) surface before attempting to construct models of the ordered Sb overlayer. The column-V elements (other than nitrogen) tend to retain their dehybridized configuration when their coordination number is 3 or less; on the GaAs(110) surface,^{20,21} the average angle between bond orbitals around the As atom is reduced from 109° to $\sim 95^\circ$. The same effect is found in simple compounds in which Sb is

triply coordinated²² (SbH_3 has bond angles of 91.6° , and SbCl_3 has bond angles of 97.2°). The general tendency of Sb to minimize its hybridization will be adopted here as a guideline.

The bond lengths will be slightly smaller than the corresponding nearest-neighbor distance in the bulk due to the lowered coordination. The percentage reduction seen of bond length in As_2 and As_4 compared to bulk As was used to calculate the Sb radius; for singly coordinated Sb, the radius $r = 1.31 \text{ \AA}$ and, for triply coordinated Sb, $r = 1.39 \text{ \AA}$. The covalent radius for As is 1.21 \AA (Ref. 23), which can be subtracted from the GaAs bond length to obtain 1.24 \AA as a covalent radius for Ga. For comparison, Pauling's covalent radius for Sb is 1.41 \AA .

The chemical nature of the GaAs(110) surface, which is determined by its electronic and atomic structure, must also be considered. The surface electronic states near the band gap will be most active in the chemistry of the (110) surface. A reconstruction occurs on the clean (110) surface such that the surface Ga atoms move 0.5 \AA toward the crystal, and the surface As atoms over 0.2 \AA away from the crystal^{24,25} [see Fig. 1(b)].

Electronically, the reconstruction alters the partially occupied “dangling-bond” states (sp^3) of the unreconstructed surface such that these states are shifted away from the band gap.^{21,26} The partially occupied “dangling-bond” state of the unreconstructed surface Ga atom shifts up in energy and becomes an empty p orbital [straight dashed lines in Fig. 1(b)], and the partially occupied “dangling-bond” state of the unreconstructed surface As atom is replaced by a doubly occupied, s -like, “lone-pair” orbital, located well below the VBM. Most important on the reconstructed surface is the empty p state on the surface Ga atoms which theory predicts is 1–2 eV above the conduction-band maximum (CBM) in energy.^{26–28} Occupied states near the VBM on the reconstructed surface, such as the p -like back bonds of the surface As atoms, are probably less dominant in the bonding (except in the case of electronegative adatoms) but should still be considered. The unreconstructed surface, on the other hand, has both Ga and As “dangling-bond” states near the band gap.

C. Structural models of the ordered Sb monolayer

Considering the strong tendency for column-V elements to form diatomic molecules and knowing that the ordered Sb monolayer has two atoms per unit cell, it is natural to think first in terms of an Sb_2 molecule bonded inside each surface unit cell. The empty p state on the Ga atom is a likely site for

bonding, but this takes care of, at most, two of the four Sb_2 electrons in π molecular orbitals, leaving two Sb_2 electrons in a weakly bound state. Based on the characteristics of the ordered Sb_2 monolayer observed experimentally, this is not a satisfactory arrangement: All electrons must be in stable (more tightly bound) states.

The As atom on the *reconstructed* surface does not have any partially filled or empty states near the band gap and thus offers no sites for bond orbitals involving the Sb electrons remaining in π molecular orbitals. If, however, the second Sb atom [denoted by Sb(2)] of the Sb_2 molecule is allowed to bridge between the Sb(1) atoms which are bonded to the Ga atom in each unit cell (assuming monolayer coverage), then each Sb atom is bonded to two other Sb atoms in a zigzag chain configuration [see Fig. 15(a)]. The Sb zigzag chain is similar to the zigzag chains of alternating Ga and As atoms on the (110) surface and, in this model (Model 1), they are superimposed [see Fig. 15(b)]. In this configuration, all Sb p electrons are in tightly bound σ -bond orbitals; Sb(1) is triply coordinated with two p electrons in the Sb(1)–Ga bond orbital and one p electron in the Sb(1)–Sb(2) bond orbitals, while Sb(2) is doubly coordinated with all three p electrons in Sb(1)–Sb(2) bond orbitals. The Sb s electrons are in tightly bound “lone-pair” orbitals.

The only constraint imposed by the GaAs lattice in this case is that the distance between Sb(1) atoms equals the distance between surface Ga atoms (4.0 Å). The zigzag chain structure accommodates this constraint perfectly; taking a bond length of 2.7 Å (shorter than the bulk bond length of 2.87 Å due to the lowered coordination) yields a 95.6° angle between bonds.

If the reconstruction of the GaAs surface lattice can be changed to an *unreconstructed* (truncated) lattice, then the Sb chain may occupy the “next-lattice-layer” sites [Model 2, see Fig. 15(c)] as an alternative configuration, with half the Sb atoms bonding to Ga and the other half bonding to As. The Sb–As bond energy may be sufficient to compensate in part for the energy required to remove the GaAs(110) reconstruction [estimated to be 1.2 eV (Ref. 20)]. In this configuration, some distortion of the sp^3 hybridization of the ideal GaAs surface lattice, along with increased hybridization of the Sb orbitals, appears necessary to form Ga–Sb and As–Sb bonds.

The zigzag chain models of the Sb overlayer are quite consistent with the characteristics determined experimentally. The chain has unit-cell dimensions and mirror symmetry like that of the substrate (1×1) with two Sb atoms per unit cell, is semiconducting (even number of electrons per unit cell), and

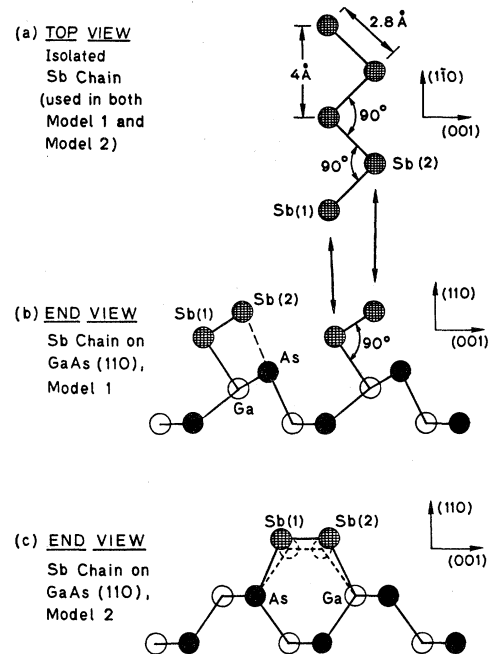


FIG. 15. Zigzag chain model for monolayer Sb adsorption on GaAs(110) at room temperature. (a) Structure of the isolated chain. Note that the chain axis is parallel to the $[1\bar{1}0]$ direction. (b) The first configuration for attachment of the Sb chain to the semiconductor lattice. The reconstruction of the GaAs surface lattice shown here is the same as that of the clean surface for the sake of illustration and will be referred to as Model 1A; an altered reconstruction is possible (see text). The correspondence between parts (a) and (b) of this figure is indicated by arrows. (c) A second configuration for attachment of the Sb chain to the surface. The GaAs surface lattice is shown completely unreconstructed to emphasize that, in this configuration, the Sb chain acts as an additional lattice layer on top of the surface layer of the GaAs. The dashed circles indicate the positions that would be taken by an additional unreconstructed or truncated GaAs lattice layer, with dashed lines along the axes of the sp^3 bond orbitals. The optimum structure of the GaAs surface lattice and the Sb overlayer may differ from the simple structure shown here (this must be determined by an energy minimization calculation or by further experiment).

is electronically stable (no nonbonding or weakly bound electrons), implying resistance to oxidation. It is clear that island formation at submonolayer coverage is energetically favorable for the chain models, in agreement with Kahn's results.¹¹ In favor of Model 2, Goddard has pointed out that the Sb valence electrons are distributed more evenly in the bridging configuration [Fig. 15(c)] as compared to the superimposed configuration [Fig. 15(b)] and that the increased coordination number of the Sb(2)

atoms in Model 2 may contribute more to the resistance of the overlayer to oxidation.²⁹

Before proceeding to calculate the electronic states associated with Models 1 and 2, it is of interest to examine the situation of lighter column-V elements on GaAs(110) in terms of a chain configuration. As the bond length (d) is decreased, the angle (θ) between bonds within the chain increases rapidly.⁹ Recalling the tendency of column-V elements to retain their dehybridized configuration, it seems likely that As or P probably shows an increased tendency to adsorb molecularly from unexcited gas phases. The results of Kübler *et al.* suggest that the observed 1×1 As overlayer is not well ordered,³⁰ which may be accounted for by either molecular adsorption with random orientation or by short distorted zigzag chain segments. It is interesting to note that the zigzag chain model can account for their results.

D. Calculated electronic states of the isolated Sb zigzag chain

The two models of the ordered Sb monolayer are both zigzag chains, differing mainly in how they are attached to the lattice. Since the Sb—Sb bond orbitals do not mix strongly with the Ga—Sb (or As—Sb) bond orbitals, and are therefore relatively independent, it will be useful to first obtain the electronic states of an isolated zigzag chain for the purpose of testing whether or not the Sb monolayer is, in fact, a zigzag chain. Second, differences arising from the site of the chain's attachment to the GaAs surface will be considered.

A tight-binding approach is used here for calculating the electronic states, employing a linear combination of atomic orbitals (LCAO) as basis states and universal matrix elements between atomic orbitals to form bond orbitals, as developed by Harrison.¹³ We may use this LCAO method first to verify the earlier statements about the greater electronic stability of a chain structure over isolated Sb₂ molecules (or single Sb atoms) within the surface unit cell. It is anticipated that the atomic orbitals most involved in bonding a single Sb atom to the GaAs(110) surface are the empty Ga p state and one of the half-filled Sb p states, based on the chemistry of the GaAs(110) surface as discussed above. The bond orbital may be doubly occupied by putting two Sb p electrons into the p state used for the bond orbital (the resulting increase in p -state energy is neglected). This leaves one Sb p electron in a nonbonding orbital above the CBM [see Fig. 16(a)], which is inconsistent with the experimental data. The end situation for an Sb₂ molecule in each unit cell is similar—once again, there are electrons in nonbond-

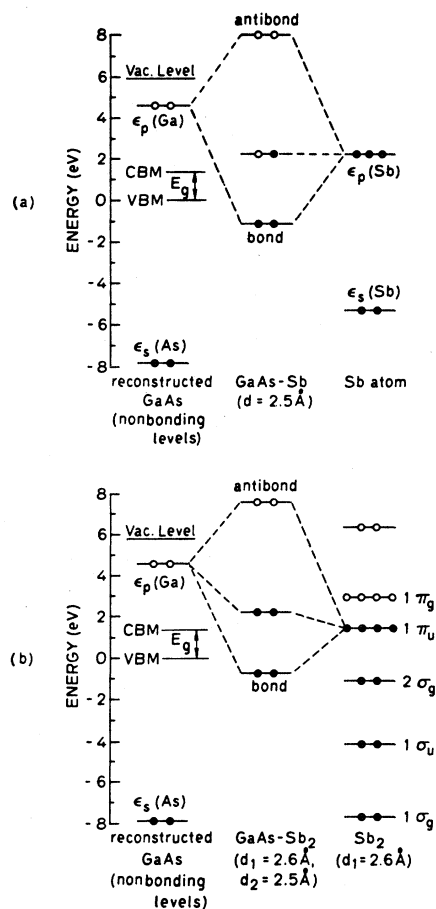


FIG. 16. Schematic representation of the orbital energies associated with (a) atomic Sb adsorbed on the Ga site and (b) Sb₂ adsorbed on the Ga site. Note that, in either case, occupied states are obtained 2 eV or more above the VBM, in sharp contrast with experimental data.

ing or weak bond orbitals [see Fig. 16(b)].

If, however, Sb₂ molecules are allowed to bond to Sb₂ molecules in adjacent unit cells along the GaAs zigzag chain (the $[1\bar{1}0]$ direction) via the p states of the other Sb₂ π orbital, an Sb zigzag chain is obtained. In effect, this creates a second $2\sigma_G$ state ~ 1 eV below the VBM (degenerate with the first). Owing to the strong coupling between states in the chain along the $[1\bar{1}0]$ direction [the chain axis, see Fig. 15(a)], some dispersion of the states is expected along this direction. The translational unit cell of the Sb chain contains two atoms and, taking advantage of the glide plane symmetry, the unit cell can be reduced to one Sb atom with only three atomic orbitals in the plane of the chain (p_x , p_y , s , or p_1 , p_2 , s , see Fig. 17).

The Hamiltonian matrix of the zigzag chain shown in Fig. 17 was constructed for electronic

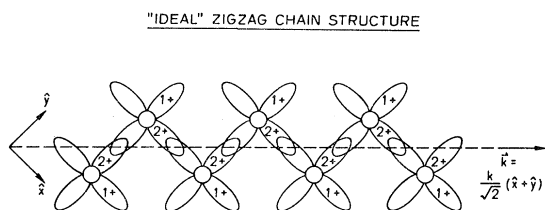


FIG. 17. Schematic representation of the atomic p states in the ideal zigzag chain structure. Note the glide plane symmetry of the p states, which is also true for the s states. Dispersion of these states was calculated for Bloch states propagating along the chain (see text). The p_z states are perpendicular to the illustrated plane.

states propagating along the chain axis (see Table I). In this matrix, ϵ_p is the atomic p -state energy, ϵ_s is the atomic s -state energy, V_{ss} is the contribution to the energy due to coupling between s states, and so on as defined by Harrison.³¹ Owing to the lack of hybridization in this simple model, the coupling between s and p states will be neglected for the first analysis. Setting V_{sp} to zero, the energy eigenvalues are

$$E(k) = \epsilon_p + 2V_{pp\pi} \cos(kd/\sqrt{2})$$

for the p_z states perpendicular to the plane of the chain,

$$E(k) = \epsilon_s + 2V_{ss} \cos(kd/\sqrt{2})$$

for the s states, and

$$E(k) = \epsilon_p \pm [V_{pp\sigma}^2 + V_{pp\pi}^2 + 2V_{pp\sigma}V_{pp\pi} \cos(\sqrt{2}kd)]^{1/2}$$

for the p_x and p_y states within the plane of the chain. Knowing that $V_{pp\pi}$ is only one-quarter as large as $V_{pp\sigma}$, we may have been tempted to ignore $V_{pp\pi}$ too, but then the $\cos(\sqrt{2}kd)$ term in the last equation would have been zero, and the strongly bonded p states in the plane of the chain would have lacked dispersion. This is because of the special

ISOLATED "IDEAL" ZIGZAG CHAIN

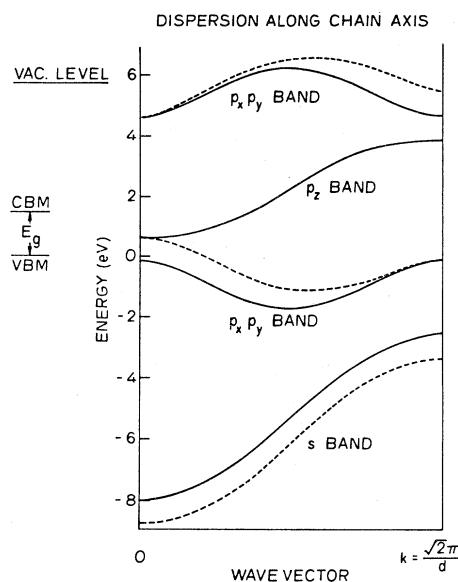


FIG. 18. Band diagram for states propagating along the zigzag chain axis. Solid lines represent neglect of sp coupling ($V_{sp}=0$), while dashed lines indicate the dispersion when sp coupling is included. The s band and lower $p_x p_y$ band are filled, while the p_z band is only half-filled.

geometry of this "ideal" zigzag chain in which the bond angles are 90° . As a result, p_x (or p_y) states couple only to p_z (or p_y) states on adjacent atoms—never to themselves. Thus as a Bloch wave function along the chain axis is constructed atom by atom, one finds that the coupling of p_x and p_y states between successive atoms is *alternately* $V_{pp\sigma}$ and then $V_{pp\pi}$. As a result, the band constructed out of the p_x and p_y states is very narrow (~ 1.6 eV, see Fig. 18) compared to the ~ 12 -eV bandwidth ($4V_{pp\sigma}$) expected for a linear chain of p states. The alternation of $V_{pp\sigma}$ and $V_{pp\pi}$ coupling is also the reason for the halved periodicity of the $p_x p_y$ band in k space compared to the s and p_z band.

TABLE I. Hamiltonian matrix of the isolated "ideal" zigzag chain for states propagating along the chain axis. $V_{11'm} = \eta_{11'm}(\hbar^2/md^2)$: $\eta_{ss} = -1.40$, $\eta_{sp} = 1.84$, $\eta_{pp\sigma} = 3.24$, $\eta_{pp\pi} = -0.81$.

$\epsilon_p + 2V_{pp\pi} \cos(kd/\sqrt{2})$	0	0	0
0	ϵ_p	$V_{pp\sigma} e^{-ikd/\sqrt{2}} + V_{pp\pi} e^{ikd/\sqrt{2}}$	$V_{sp} e^{-ikd/\sqrt{2}}$
0	$V_{pp\sigma} e^{ikd/\sqrt{2}} + V_{pp\pi} e^{-ikd/\sqrt{2}}$	ϵ_p	$-V_{sp} e^{ikd/\sqrt{2}}$
0	$V_{sp} e^{ikd/\sqrt{2}}$	$-V_{sp} e^{-ikd/\sqrt{2}}$	$\epsilon_s + 2V_{ss} \cos(kd/\sqrt{2})$

The neglect of sp coupling may have strong consequences for the dispersion relations; therefore, it is important to see the effect of including the sp coupling ($V_{sp} \neq 0$). The numerical solution is shown with dashed lines in Fig. 18, from which it is clear that the change in dispersion due to the inclusion of sp coupling is a relatively small perturbation on the dispersion without sp coupling. The $p_x p_y$ bands, now with some s character, no longer have the halved Brillouin zone of the translational unit cell, and the p_z band is unaffected since the p_z states are orthogonal to the s states.

E. Calculated electronic states of the Sb—GaAs bonds

The bonding of the chain to a (110) surface lattice should be considered next. In considering the states associated with the bonding of the Sb chain to GaAs, what amounts to a cluster calculation is done, which ignores the dispersion of the electronic states. The simplest scheme is to use the attachment configuration of Model 1 [Fig. 15(b)], since then it is mainly the p_z states of the chain and the empty Ga p states which are involved in the bonding of the chain to the (110) surface. With the use of only the Ga and Sb p states, and a bond length of 2.63 Å, a bond orbital is obtained at -0.3 eV (below the GaAs VBM) and an antibond orbital is obtained at $+7.2$ eV (above the GaAs VBM). Including the Ga s state, states at -3.0 eV (mainly the Ga s state), $+0.7$ eV (mainly the p bond orbital), and $+7.4$ eV (mainly the p antibond orbital) are obtained. Thus a Ga—Sb p -like bond orbital near the VBM is expected with the attachment scheme of Model 1. With no change in the GaAs surface lattice, there is strong overlap between the p state of the essentially dehybridized surface As atom (which bonds to a

second-layer Ga atom) and the empty Sb(2) p state [see dashed line in Fig. 15(b)]. With the use of only p states on Sb and As and an sp^3 hybrid on the Ga, the energy of the As back-bond state is lowered by ~ 1.4 eV from -2.5 to -3.9 eV, mainly due to a lowered average energy of the states involved.

In the case of complete removal of the GaAs(110) reconstruction in Model 1, the nonbonding states on the surface As and Ga atoms have sp^3 character, and the Sb chain interacts principally with the Ga sp^3 "dangling bond." The Ga—Sb bond orbital is then ~ -1.5 eV below the VBM ($d=2.63$ Å). With the removal of the GaAs reconstruction, the GaAs surface electronic states are altered: All Ga—As bonds are now constructed from sp^3 states, with energy ~ 4.8 eV below the VBM (ignoring dispersion), and the surface As nonbonding orbital is now a sp^3 "dangling bond" ~ 0.8 eV below the VBM. The Model-1 attachment configuration with a reconstructed GaAs lattice will be referred to as Model 1A and with the unreconstructed GaAs lattice as Model 1B.

For simplicity in calculating the states associated with Model 2, the symmetric structure illustrated in Fig. 15(c) is used, assuming complete removal of the GaAs surface lattice reconstruction. Pure p states on the Sb atoms and pure sp^3 hybrids on the surface Ga and As atoms were used as a first approximation. In this case, a bond energy 1.5 eV below the VBM is again obtained for the Ga—Sb bond and 3.7 eV below the VBM for the As—Sb bond. These results are summarized in Table II.

F. Comparison of calculated states and photoemission EDC's

In the interest of simplicity, an imprecise but easily applied method was used to calculate the electron-

TABLE II. Summary of calculated energies.

Zigzag chain (isolated)	Sb—Sb p -like band between -1 and $+0.5$ eV Sb—Sb s -like band between -9 and -3.5 eV
Model 1A (GaAs fully reconstructed)	Ga—Sb bond centered at $+0.7$ eV As back-bond shifts from -2.5 to -3.9 eV due to Sb
Model 1B (GaAs unreconstructed)	Ga—Sb bond centered at -1.5 eV As back-bond shifts from -2.5 to -4.8 eV As "dangling bond" centered at -0.8 eV
Model 2 (symmetric, GaAs unreconstructed)	Ga—Sb bond centered at -1.5 eV As—Sb bond centered at -3.7 eV Ga—As bonds more bulklike

ic states. As an indication of the magnitude of the errors in this method, the energy of bond orbitals was compared with and without inclusion of s - p coupling (V_{sp}). In the case of the Sb—Sb or Ga—Sb bonds, this resulted in a shift in the bond-orbital energies of $\lesssim 1.0$ eV. Thus the calculated energies of the states are probably only correct to within 1 eV. Nonetheless, the calculated energies are very useful in interpreting the data.

First, the data should be reexamined to see if the calculated states obtained from the zigzag chain configuration (see Table II) are consistent with the Sb-induced structure of the EDC's. From the model calculations, it was found that the zigzag chain has four of the six Sb p electrons per unit cell in Sb—Sb bond orbitals which form a narrow p -like band between -1 and $+0.5$ eV (see Table II). The p electrons have a strong photoemission cross section in this photon energy range, and it is therefore concluded that the dominant angle-integrated emission from a zigzag Sb chain would be from the Sb—Sb bonds near the VBM. The p -like doubly occupied Sb—Ga bond also falls into the same region in energy ($+0.7$ eV for Model 1A and -1.5 eV for Models 1B and 2; see Table II) and will contribute some additional emission near the VBM.

In fact, as shown in Figs. 8, 9, and 11–13, the predominant new emission associated with submonolayer Sb deposition was a peak centered at -0.5 eV (see Fig. 9). For this reason, the prominent peak centered at -0.5 eV in the 0.3 ML Sb difference curves is associated with the Sb—Sb bonds of the zigzag chain, with the possibility that the Sb—Ga bonds may also contribute to the peak.

Before the zigzag chain model can be accepted, it remains to be considered why the -0.5 -eV peak does not display any obvious dependence on photon energy (i.e., dispersion) or on angle-resolved PES orientation. The parallel component of the initial-state wave vector for the -0.5 -eV peak increases from 0.9 to 1.2 \AA^{-1} in the photon energy range 21–28 eV. Owing to the small bandwidth (~ 1.6 eV), together with the expanded unit cell of the Sb chain (see Fig. 18), variations in peak position with photon energy in the range 21–28 eV are therefore expected to be slight. Thus the almost negligible (~ 0.15 eV) change observed in peak position within this photon energy range is not surprising. Perhaps more importantly, the submonolayer Sb islands observed by Carelli and Kahn¹¹ were thought to be in the range of 10 to 100 \AA diameter. At 0.3 ML coverage, the average island diameter was probably near the low end of this range and the extended nature of the chain's electronic states lost. In this situation, both dispersion and variation in azimuthal emission may be greatly reduced due to nonextended initial

states and nonconservation of momentum parallel to the surface (see, for example, Ref. 32).

The analysis of other features in the photoemission data relates more to the attachment scheme of the Sb chain to the surface rather than to the Sb chain itself. First, a strong loss in emission from the GaAs states ~ 2 eV below the VBM occurred following deposition of one or more monolayers of Sb (see Fig. 8). Theoretical calculations of the GaAs(110) surface electronic states have predicted two states near this energy: an As "back-bond" state and a mixed first- and second-layer state which is mainly As p -like.^{26–28} The strong perturbation of this state is consistent with a change in the GaAs surface lattice reconstruction and/or bonding of Sb to As in the surface lattice as described above. Second, the GaAs(110) surface excitonic transition, which is thought to be localized at the surface Ga atoms,¹⁸ is removed (not shifted) by Sb deposition. This may or may not be due to a change in GaAs surface lattice reconstruction but would be expected with the bonding of Sb to Ga in the surface lattice. Third, weaker Sb-induced structure was observed in photoemission difference curves between -2 and -4 eV. Each of the attachment schemes for the zigzag chain model described earlier was expected to have these effects (see Table II) and, although it is possible to conclude that both Ga- and As-derived states are strongly perturbed, these data cannot distinguish between the attachment schemes. Fourth, the data showed an increase in average yield of the normalized angle-resolved PES emission above the VBM of $\sim 34\%$ in going from orientation 2 to orientation 4. This result can easily be accounted for by a contribution to the emission above the VBM from the Ga—Sb bonds as predicted by the calculations above (see Table II). Recently, however, calculated LEED I - V profiles³³ for both Models 1 and 2 have been compared to experimental data for an Sb monolayer on GaAs(110). Poor results were obtained for the Model-1 attachment scheme, but very good results were obtained for a slightly asymmetric Model 2 (with reliability factor $R = 0.19$).

V. SUMMARY AND CONCLUSIONS

The nature of Sb overlayers on GaAs(110) has been characterized by photoemission and LEED. Sb forms an ordered monolayer which bonds strongly to the GaAs and is chemically quite stable against oxidation. Several models for the ordered Sb monolayer were considered. A zigzag chain configuration was found to be the most consistent with the feature of stability and had electronic states that were quite consistent with the data (the single atom or Sb₂ molecule models were inconsistent with the data). From

the lack of dispersion of the Sb-induced states in the photoemission data at low (0.3 ML) coverage, it may be concluded that island formation does indeed occur at submonolayer coverage, as earlier reported by Carelli and Kahn.¹¹ Furthermore, the island size at 0.3 ML coverage may be quite small—again, due to the lack of dispersion in the Sb-induced states.

The calculational techniques³¹ used here, though imprecise, were extremely useful for identifying the basic character of the electronic states associated with the overlayer. The use of such a simple theoretical approach greatly increases the ability of the experimentalist to properly interpret his data.

A very easy approach to determine which of the two attachment schemes (Models 1 and 2) for the zigzag chain is correct would be to do a LEED experiment on Ge(110) instead of GaAs(110). Owing to the slight ionicity of GaAs, the zigzag chain is likely to be asymmetric (rotated) with respect to the surface plane even in the case of a Model-2 attachment scheme. However, the Model-2 scheme, if correct, should be symmetric with respect to the Ge(110) surface and all (10) diffraction beams should be extremely weak or disappear.¹⁰

The zigzag chain model also hints at why the (110) surface of GaAs has never been particularly favorable for growth by molecular-beam epitaxy. The Sb zigzag chain structure is quite stable chemically and, while an As overlayer may not form along continuous chains, it may still be quite stable, thus inhibiting growth (this could lead to faceting).

Lastly, this system [column-V elements on GaAs(110) surface] is in need of more theoretical analysis. Total energy calculations would be useful

for comparing the two models and for determining the reconstruction of the GaAs(110) surface lattice with an Sb chain adsorbed. A more careful determination of the electronic states associated with the chain on the surface would be of obvious importance in relation to angle-resolved photoemission measurements of Sb on GaAs(110) or Ge(110).

ACKNOWLEDGMENTS

One of us (P.S.) would especially like to thank Professor Goddard (California Institute of Technology) for pointing out several important features of Model 2 which caused us to reconsider this attachment scheme for the zigzag chain (we had earlier thought that the large angle between bonds in Model 2 was a serious fault). The authors have greatly enjoyed collaboration and several discussions with Professor Kahn (Princeton University). The members of the Tube Lab at Stanford, who, on our behalf, often modified or fixed the equipment on short notice, are greatly appreciated. This work was supported by the U. S. Office of Naval Research (ONR) under Contract No. N00014-75-C-0289 and by the Advanced Research Projects Agency of the U. S. Department of Defense (monitored by ONR) under Contract No. N00014-79-C-0072. Part of this work was performed at the Stanford Synchrotron Radiation Laboratory (SSRL) which is supported by the National Science Foundation, Grant No. CMR-73-07692, in cooperation with the Stanford Linear Accelerator Center and the U. S. Department of Energy.

*Present address: Bell Laboratories, 600 Mountain Avenue, Murray Hill, New Jersey 07974.

†Present address: Hewlett-Packard Corp., 1501 Page Mill Road, Palo Alto, California 94306.

¹I. Lindau and W. E. Spicer, in *Synchrotron Radiation Research*, edited by H. Winick and S. Doniach (Plenum, New York, 1980), and references therein.

²P. Pianetta, I. Lindau, P. E. Gregory, C. M. Garner, and W. E. Spicer, *Surf. Sci.* **72**, 298 (1978).

³A. Y. Cho and J. R. Arthur, *Prog. Solid State Chem.* **10**, 157 (1975).

⁴R. Z. Bachrach, *Prog. Cryst. Growth Character* **2**, 115 (1979).

⁵S. Doniach, I. Lindau, W. E. Spicer, and H. Winick, *J. Vac. Sci. Technol.* **12**, 1123 (1975).

⁶P. Skeath, W. A. Saperstein, P. Pianetta, I. Lindau, W. E. Spicer, and P. Mark, *J. Vac. Sci. Technol.* **15**, 1219 (1978).

⁷P. Skeath, I. Lindau, P. W. Chye, C. Y. Su, and W. E. Spicer, *J. Vac. Sci. Technol.* **16**, 1143 (1979).

⁸W. E. Spicer, in *Electron and Ion Spectroscopy of Solids*, edited by L. Fiermans, J. Vennik, and W. DeKeyser (Plenum, New York, 1978).

⁹P. Skeath, C. Y. Su, I. Lindau, and W. E. Spicer, *J. Vac. Sci. Technol.* **17**, 874 (1980).

¹⁰A. U. MacRae and G. W. Gobeli, *J. Appl. Phys.* **35**, 1639 (1964).

¹¹J. Carelli and A. Kahn, *Surf. Sci.* **116**, 380 (1982).

¹²D. E. Eastman, T.-C. Chiang, P. Heimann, and F. J. Himpsel, *Phys. Rev. Lett.* **45**, 656 (1980).

¹³C. Y. Su, I. Lindau, P. W. Chye, P. R. Skeath, and W. E. Spicer, *Phys. Rev. B* **25**, 4045 (1982).

¹⁴P. Pianetta, I. Lindau, C. M. Garner, and W. E. Spicer, *Phys. Rev. B* **18**, 2792 (1978).

¹⁵Y. L. Yarnell, J. L. Warren, R. G. Wenzel, and S. H. Koenig, *IBM J. Res. Dev.* **8**, 234 (1964).

¹⁶T. S. Moss, *Photoconductivity of the Elements* (Butterworth, Washington, D.C., 1952).

¹⁷J. van Laar, A. Huijser, and T. L. van Rooy, *J. Vac. Sci. Technol.* **16**, 1164 (1979).

- ¹⁸G. J. Lapeyre and J. Anderson, Phys. Rev. Lett. 35, 117 (1975).
- ¹⁹G. J. Lapeyre, R. J. Smith, and J. Anderson, J. Vac. Sci. Technol. 14, 384 (1977).
- ²⁰C. A. Swarts, W. A. Goddard, and T. C. McGill, J. Vac. Sci. Technol. 17, 982 (1980); 19, 360 (1981).
- ²¹W. A. Harrison, Surf. Sci. 55, 1 (1976).
- ²²*Landolt-Börnstein*, edited by K. H. Hellwege (Springer, Berlin, 1976), New Series, Group II, Vol. 7.
- ²³L. Pauling, *The Nature of the Chemical Bond*, 3rd ed. (Cornell University Press, Ithaca, 1960).
- ²⁴A. Kahn, E. So, P. Mark, C. B. Duke, and R. J. Meyer, J. Vac. Sci. Technol. 15, 1223 (1978).
- ²⁵S. Y. Tong, A. R. Lubinsky, B. J. Mrstik, and M. A. van Hove, Phys. Rev. B 17, 3303 (1978).
- ²⁶D. J. Chadi, Phys. Rev. B 18, 1800 (1978).
- ²⁷A. Zunger, Phys. Rev. B 22, 959 (1980).
- ²⁸J. R. Chelikowsky, S. G. Louie, and M. L. Cohen, Solid State Commun. 20, 641 (1976).
- ²⁹W. A. Goddard (private communication).
- ³⁰B. Kübler, W. Ranke, and K. Jacobi, Surf. Sci. 92, 519 (1980).
- ³¹W. A. Harrison, *Electronic Structure and the Properties of Solids* (Freeman, San Francisco, 1980).
- ³²N. J. Shevchik, Phys. Rev. B 16, 3428 (1977).
- ³³C. B. Duke, A. Paton, W. Ford, A. Kahn, and J. Carelli, Phys. Rev. B 26, 803 (1982).